Catalysis Today xxx (2016) xxx–xxx

Contents lists available at ScienceDirect

Catalysis Today

journal homepage: www.elsevier.com/locate/cattod

Catalytic water splitting

Synthetically tunable iridium(III) bis-pyridine-2-sulfonamide complexes as efficient and durable water oxidation catalysts

Mo Li, Stefan Bernhard*

Department of Chemistry, Carnegie Mellon University, Pittsburgh, PA, 15213, USA

ARTICLE INFO

Article history:
Received 25 August 2016
Received in revised form 4 November 2016
Accepted 7 November 2016
Available online xxx

Keywords:
Water oxidation
Iridium bpsa complex
Tunability
Electronic structure
HOMO energy

ABSTRACT

A series of phenylene-linked iridium bis-pyridine-2-sulfonamide (bpsa) complexes substituted with electron-donating and electron-withdrawing groups and a new bpsa complex containing naphthalene linkage were synthesized and investigated as efficient and robust water oxidation catalysts. It was found that the oxidation potentials of these substituted complexes are within a broad range, which reflects their effectively tuned electronic structures. Under various water oxidation conditions, diverse kinetics behaviors are observed. The reaction mechanism strongly depends on the structure of the catalyst, and the nature of the oxidant as well as their ratios and concentrations. As evidenced by cyclic voltammetry and DFT calculations, the addition of electron-donating substituents greatly destabilizes the HOMO of the catalyst and thus facilitates the initial oxidation process. On the other hand, the limited driving force provided by the oxidized state of an electron-rich catalyst also impedes efficient water oxidation reactions. The robustness of a water oxidation catalyst is critical, and long-term reactions have exhibited turnover numbers (TONs) of up to 16,200.

© 2016 Elsevier B.V. All rights reserved.

1. Introduction

The constantly growing demand for energy has trigged intensive and wide-spread research to discover sustainable solar energy conversion strategies [1–6]. The probably most attractive solution is the storage of solar energy in chemical bonds to fuels [7–11]. For all the potential artificial photosynthetic systems such as water splitting [12–17], carbon dioxide reduction [18–21] and photobiological production of fuels [22,23], the complementary oxidative half-reaction is critical. A desirable oxidative process that can be coupled to various reductive pathways for fuel production is the production of molecular oxygen from water, an abundant and benign feedstock. Besides, the direct use of atmospheric O_2 in fuel cell or combustion applications makes water oxidation an appealing goal, rendering it superior to many other currently studied oxidative processes such as halogenide oxidation [24,25] and alcohol dehydrogenation [26,27]. Significant efforts have been devoted on developing water oxidation catalysts, great challenges still remain for overcoming the vast energy barrier and the inherent complexity of orchestrating the sequential steps of transferring four electrons and four protons per molecule of formed oxygen.

The advantages of numerous characterization methods available in homogeneous system and the synthetic tunability of the ligand structure render molecular water oxidation catalysis an appealing target [28,29]. Early work on transition metal water oxidation catalysts (WOCs) focused on di- and tetrametallic complexes [30–36], making use of the metal-metal cooperativity to reduce the redox demand on each metal center. As more and more single site catalysts with well-designed ligand framework have been reported more recently [37–60], it has been well accepted that the presence of linked metal centers is not required. Among these monometallic complexes, iridium-based WOCs are of great interest because of their remarkable water oxidation reactivity and robustness under the harsh oxidizing environments required for driving these reactions.

Up to date, cyclometalated iridium phenylpyridine complexes [42], half-sandwich iridium Cp* (Cp* = pentamethylcyclopentadienyl) complexes [43,44,47,48,61], iridium carboxylates [62,63] and recently reported wrap-around iridium bis-pyridine-2-sulfonamide (bpsa) complexes [49] represent some of the major classes of efficient iridium-based WOCs. A variety of iridium Cp* complexes with diverse ligand systems have been shown to catalyze water oxidation with extraordinarily high activities compared to the iridium phenylpyridine complexes. However, several degradation pathways of the Cp* ligand leading to structural modifications or even complete loss of the Cp* ligand have been documented, which can trigger concerns of molecular catalyst transforming into active colloids [64–68]. Careful dynamic light scattering (DLS) studies [48,49,69] have confirmed the molecular nature of some catalysts, but illuminating the mechanism

* Corresponding author.
E-mail address: bern@cmu.edu (S. Bernhard).

http://dx.doi.org/10.1016/j.cattod.2016.11.027
0920-5861/© 2016 Elsevier B.V. All rights reserved.

Please cite this article in press as: M. Li, S. Bernhard, Synthetically tunable iridium(III) bis-pyridine-2-sulfonamide complexes as efficient and durable water oxidation catalysts, Catal. Today (2016), http://dx.doi.org/10.1016/j.cattod.2016.11.027

involved in water oxidation reaction catalyzed by a variety of emerging species is difficult and such a transformation greatly hinders the development of solar fuel systems.

The newly designed iridium bpsa complexes supported by a resilient wrap-around ligand platform effectively addressed the ligand instability issues, demonstrating remarkably stable performance in water oxidation [49]. Electrochemical quartz crystal microbalance (EQCM) and dynamic light scattering (DLS) experiments conclusively ruled out the formation of active IrO_x nanoparticles [49]. The robust structure of bpsa ligand framework, capable to stabilize the high valent metal oxo intermediates formed during water oxidation through extended charge delocalization, offers a promising direction in future catalysts design.

Based on our previous work on these iridium bpsa complexes [49], systematic modification of the sulfonamide linker moiety (Fig. 1) allowed the synthetic tuning of the electronic properties of these complexes. Phenylene-linked bpsa ligands with electron-donating and electron-withdrawing groups as well as a new bpsa ligand H_2bpsa-NPTH with naphthalene linkage were synthesized and used to prepare the corresponding iridium complexes **1**-**5** (Fig. 1). The catalytic performance of these substituted iridium bpsa complexes were evaluated under various conditions, highlighting the robustness and efficiency of these systems. Through cyclic voltammetry and DFT calculations, the electronic properties of these complexes were explored, which implicitly illustrates the effect of the different substituents on the ability to catalyze water oxidation.

2. Experimental

2.1. Materials

2-Mercaptopyridine, sodium hypochlorite (14.5%), 1,2-phenylenediamine, 4,5-dichloro-1,2-phenylenediamine, 4,5-difluoro-1,2-phenylenediamine, 4,5-dimethyl-1,2-phenylenediamine, 2,3-diaminonaphthalene and all solvents were obtained from commercial sources and used without further purification. $IrCl_3 \cdot xH_2O$ was purchased from Pressure Chemical Co. and used as received.

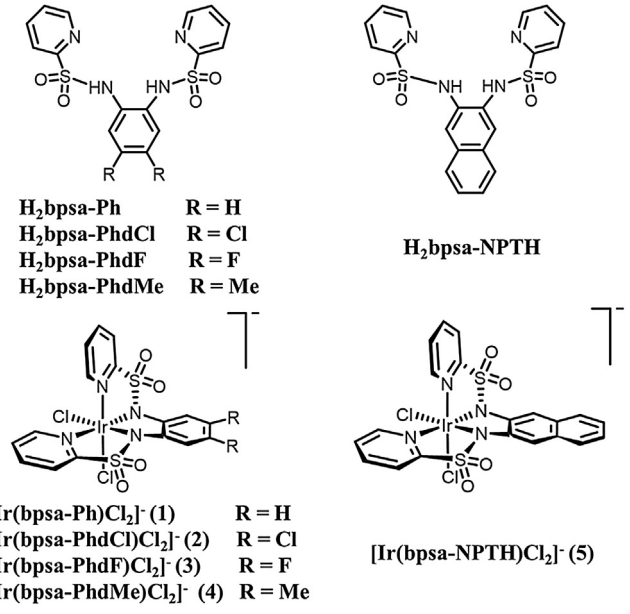

Fig. 1. Schematic structures of bis-pyridine-2-sulfonamide ligands H_2bpsa-Ph, H_2bpsa-PhdCl, H_2bpsa-PhdF, H_2bpsa-PhdMe, H_2bpsa-NPTH (top) and the corresponding Ir(III) complexes $[Ir(bpsa\text{-}Ph)Cl_2]^-$ **1**, $[Ir(bpsa\text{-}PhdCl)Cl_2]^-$ **2**, $[Ir(bpsa\text{-}PhdF)Cl_2]^-$ **3**, $[Ir(bpsa\text{-}PhdMe)Cl_2]^-$ **4**, $[Ir(bpsa\text{-}NPTH)Cl_2]^-$ **5** (bottom). All the complexes exhibit C_1 symmetry as characterized by NMR spectroscopy, which is in agreement with the geometry observed for the previously published parent complex **1** [49].

2.2. Complexes synthesis

2.2.1. Synthesis of pyridine-2-sulfonyl chloride

Pyridine-2-sulfonyl chloride was prepared according to the previously published procedure [49]. Typically, a solution of 2-mercaptopyridine (3.24 g, 29.2 mmol) in 20 mL dichloromethane was combined with concentrated hydrochloric acid (81 mL), and the mixture was cooled to 0 °C in an ice bath. Sodium Hypochlorite (14.5%, 178 mL) was added dropwise and the reaction mixture which turned yellow gradually was stirred for another 30 min at 0 °C. The resulting solution mixture was extracted twice with dichloromethane (~30 mL), and the organic layers were combined and dried over sodium sulfate for half an hour. The solid was filtered off, and the solvent was mostly removed in a rotary evaporator, yielding a colorless liquid (~3 mL). The resulting pyridine-2-sulfonyl chloride solution was immediately used for preparing the following bis(pyridine-2-sulfonamide) ligands with various substituents due to its moderate stability in the presence of air or water. Yield: 74%. ^{1}H NMR (500 MHz, $CDCl_3$): δ 8.84 (d, J = 4.5 Hz, 1H), 8.13 (d, J = 7.7 Hz, 1H), 8.07 (td, J = 7.3, 1.5 Hz, 1H), 7.71 (ddd, J = 7.1, 4.8, 1.3 Hz, 1H), 5.30 (s, dichloromethane).

2.2.2. Synthesis of bis(pyridine-2-sulfonamide) (bpsa) ligands

Following a modified procedure based on the method described in the previous work [49], the appropriate diamine (0.5 equiv) was added slowly to a solution of the colorless pyridine-2-sulfonyl chloride resulting from previous steps in 10 mL pyridine, which was cooled to 0 °C in an ice bath. The resulting mixture was stirred overnight while it gradually warmed up to room temperature. A large amount of precipitate was formed upon slow addition of purified water to the reaction mixture. The precipitate was collected via vacuum filtration and washed with diethyl ether. The crude product was dissolved in minimal amount of hot ethanol, and then was stored in a refrigerator overnight for crystallization.

N,*N*′-(1,2-phenylene)bis(pyridine-2-sulfonamide) (H_2bpsa-Ph). Yield: 67.4%, white crystals. ^{1}H NMR (500 MHz, $CDCl_3$): δ 10.37 (s, 2H), 8.77 (d, J = 4.9 Hz, 2H), 8.07 (td, J = 7.9, 1.0 Hz, 2H), 8.00 (dt, J = 7.9, 1.6 Hz, 2H), 7.59 (ddd, J = 7.6, 4.9, 1.0 Hz, 2H), 7.56 (dd, J = 6.0, 3.6 Hz, 2H), 7.21 (dd, J = 6.1, 3.5 Hz, 2H). ^{13}C NMR (125 MHz, $CDCl_3$): δ 157.5, 148.4, 139.6, 130.2, 127.8, 127.7, 127.4, 122.7. ESI–MS (m/z, 1% trifluoroacetic acid in MeOH): 413.1 (100%, H_2bpsa-Ph-Na^+), 391.1 (50%, H_2bpsa-Ph).

N,*N*′-(4,5-dichloro-1,2-phenylene)bis(pyridine-2-sulfonamide) (H_2bpsa-PhdCl). Yield: 48.2%, white crystals. ^{1}H NMR (500 MHz, $CDCl_3$): δ 10.41 (s, 2H), 8.75 (d, J = 4.9 Hz, 2H), 8.09 (td, J = 7.9, 0.9 Hz, 2H), 8.05 (dt, J = 7.8, 1.6 Hz, 2H), 7.68 (s, 2H), 7.63 (ddd, J = 7.4, 4.9, 1.3 Hz, 2H). ^{13}C NMR (125 MHz, $CDCl_3$): δ 157.1, 148.7, 139.9, 131.7, 129.7, 129.0, 127.7, 122.8. ESI–MS (m/z, 1% trifluoroacetic acid in MeOH): 480.9 (100%, H_2bpsa-PhdCl-Na^+), 458.9 (74%, H_2bpsa-PhdCl).

N,*N*′-(4,5-difluoro-1,2-phenylene)bis(pyridine-2-sulfonamide) (H_2bpsa-PhdF). Yield: 26.8%, brown crystals. ^{1}H NMR (500 MHz, $CDCl_3$): δ 10.41 (s, 2H), 8.75 (d, J = 4.8 Hz, 2H), 8.09 (td, J = 7.8, 0.9 Hz, 2H), 8.04 (dt, J = 7.8, 1.5 Hz, 2H), 7.63 (ddd, J = 7.4, 4.9, 1.3 Hz, 2H), 7.42 (t, J = 9.3 Hz, 2H). ^{13}C NMR (125 MHz, $CDCl_3$): δ 157.1, 148.7, 139.9, 127.7, 126.6, 122.8, 116.6, 116.5. ESI–MS (m/z, 1% trifluoroacetic acid in MeOH): 449.0 (100%, H_2bpsa-PhdF-Na^+), 427.0 (58%, H_2bpsa-PhdF).

N,*N*′-(4,5-dimethyl-1,2-phenylene)bis(pyridine-2-sulfonamide) (H_2bpsa-PhdMe). Yield: 81.8%, off-white crystals. ^{1}H NMR (500 MHz, $CDCl_3$): δ 10.22 (s, 2H), 8.76 (d, J = 4.6 Hz, 2H), 8.06 (d, J = 7.9 Hz, 2H), 7.99 (dt, J = 7.8, 1.5 Hz, 2H), 7.58 (dd, J = 7.6,

Please cite this article in press as: M. Li, S. Bernhard, Synthetically tunable iridium(III) bis-pyridine-2-sulfonamide complexes as efficient and durable water oxidation catalysts, Catal. Today (2016), http://dx.doi.org/10.1016/j.cattod.2016.11.027

4.9 Hz, 2H), 7.30 (dd, J = 15.2, 1.3 Hz, 2H), 1.59 (s, 2H). ^{13}C NMR (125 MHz, $CDCl_3$): δ 157.5, 148.7, 139.5, 136.7, 128.5, 127.5, 127.3, 122.8, 19.4. ESI–MS (m/z, 1% trifluoroacetic acid in MeOH): 441.0 (100%, H_2bpsa-PhdMe-Na$^+$), 418.9 (57%, H_2bpsa-PhdMe).

N,*N*′-(naphthalene-2,3-diyl)bis(pyridine-2-sulfonamide) (H_2bpsa-NPTH). Yield: 36.9%, brown crystals. ^{1}H NMR (500 MHz, $CDCl_3$): δ 10.46 (s, 2H), 8.79 (d, J = 4.9 Hz, 2H), 8.07 (td, J = 7.9, 0.9 Hz, 2H), 8.04 (s, 2H), 7.98 (dt, J = 7.8, 1.7 Hz, 2H), 7.78 (dd, J = 6.2, 3.2 Hz, 2H), 7.58 (ddd, J = 7.6, 4.9, 1.0 Hz, 2H), 7.44 (dd, J = 6.3, 3.2 Hz, 2H). ^{13}C NMR (125 MHz, $CDCl_3$): δ 157.5, 148.8, 139.5, 132.1, 128.3, 127.7, 127.5, 126.7, 126.4, 122.9. ESI–MS (m/z, 1% trifluoroacetic acid in MeOH): 463.0 (100%, H_2bpsa-NPTH-Na$^+$), 441.0 (60%, H_2bpsa-NPTH).

2.2.3. Synthesis of iridium(III) bis(pyridine-2-sulfonamide) (bpsa) complexes

Ir(III) bpsa complexes were synthesized by modifying the previously published procedure [49]. Typically, $IrCl_3{\cdot}xH_2O$ (0.10 g, 0.28 mmol), 1 equiv of appropriate H_2bpsa ligand (0.28 mmol), and 8/1 (v/v) 2-methoxyethanol/water (~27 mL) were combined in a sealed round-bottom flask and degassed with argon for 15 min. The mixture was heated at 110 °C in the dark under an argon atmosphere for 2 h, and the solvent was removed in a rotary evaporator after the reaction mixture was cooled to room temperature. The desired Ir(III) bpsa complex was purified by chromatography on silica gel using 2/1 (v/v) ethyl acetate/acetone eluent, yielding a yellow powder after drying in the vacuum oven.

Iridium *N*,*N*′-(phenylene-1,2-diyl)bis(pyridine-2-sulfonamide) dichloride sodium salt (Na[Ir(bpsa-Ph)Cl_2]) **1**. Yield: 35.3%, yellow powder. ^{1}H NMR (500 MHz, acetone-d_6): δ 9.70 (dd, J = 6.3, 1.5 Hz, 1H), 8.40 (dt, J = 7.9, 1.5 Hz, 1H), 8.05 (m, 2H), 7.92 (m, 2H), 7.77 (d, J = 7.9 Hz, 1H), 7.51 (dd, J = 8.0, 1.4 Hz, 1H), 7.45 (ddd, J = 7.6, 6.0, 1.5 Hz, 1H), 7.27 (dd, J = 8.0, 1.3 Hz, 1H), 6.79 (dt, J = 7.8, 1.5 Hz, 1H), 6.67 (dt, J = 7.8, 1.5 Hz, 1H). ^{13}C NMR (125 MHz, D_2O): δ 162.3, 161.4, 150.9, 150.8, 142.2, 141.5, 140.4, 130.6, 129.5, 128.9, 125.9, 125.7, 125.2, 122.0, 117.1, 97.3. ESI–MS (m/z, MeOH): 650.1 (100%, [Ir(bpsa-Ph)Cl_2]$^-$).

Iridium *N*,*N*′-(4,5-dichloro-phenylene-1,2-diyl)bis(pyridine-2-sulfonamide) dichloride sodium salt (Na[Ir(bpsa-PhdCl)Cl_2]) **2**. Yield: 29.7%, dark yellow powder. ^{1}H NMR (500 MHz, CD_3CN): δ 9.73 (dd, J = 5.6, 1.2 Hz, 1H), 8.26 (dt, J = 7.9, 1.4 Hz, 1H), 7.97 (dt, J = 7.7, 1.2 Hz, 1H), 7.90 (m, 2H), 7.85 (ddd, J = 7.8, 5.7, 1.4 Hz, 1H), 7.78 (d, J = 7.8 Hz, 1H), 7.46 (s, 1H), 7.42 (s, 1H), 7.35 (ddd, J = 13.4, 7.7, 1.4 Hz, 1H). ^{13}C NMR (125 MHz, D_2O): δ 161.7, 158.1, 151.1, 150.9, 144.6, 142.4, 141.6, 140.6, 130.6, 129.6, 128.9, 127.4, 125.9, 125.2, 123.4, 117.7. ESI–MS (m/z, MeOH): 720.9 (100%, [Ir(bpsa-PhdCl)Cl_2]$^-$).

Iridium *N*,*N*′-(4,5-difluoro-phenylene-1,2-diyl)bis(pyridine-2-sulfonamide) dichloride sodium salt (Na[Ir(bpsa-PhdF)Cl_2]) **3**. Yield: 27.7%, dark yellow powder. ^{1}H NMR (500 MHz, CD_3CN): δ 9.73 (dd, J = 5.7, 1.0 Hz, 1H), 8.26 (dt, J = 7.8, 1.4 Hz, 1H), 7.96 (dt, J = 7.8, 1.2 Hz, 1H), 7.90 (m, 2H), 7.84 (ddd, J = 7.7, 5.7, 1.4 Hz, 1H), 7.76 (d, J = 7.9 Hz, 1H), 7.34 (ddd, J = 7.6, 5.8, 1.4 Hz, 1H), 7.27 (dd, J = 12.2, 8.0 Hz, 1H), 7.23 (dd, J = 12.3, 8.4 Hz, 1H). ^{13}C NMR (125 MHz, D_2O): δ 161.7, 158.1, 151.2, 151.0, 142.3, 141.6, 130.6, 129.6, 125.8, 125.2, 116.4, 116.2, 105.1, 104.9. ESI–MS (m/z, MeOH): 687.0 (100%, [Ir(bpsa-PhdF)Cl_2]$^-$).

Iridium *N*,*N*′-(4,5-dimethyl-phenylene-1,2-diyl)bis(pyridine-2-sulfonamide) dichloride sodium salt (Na[Ir(bpsa-PhdMe)Cl_2]) **4**. Yield: 34.3%, yellow powder. ^{1}H NMR (500 MHz, CD_3CN): δ 9.72 (dd, J = 5.7, 1.5 Hz, 1H), 8.24 (dt, J = 7.8, 1.5 Hz, 1H), 7.92 (dt, J = 7.7, 1.4 Hz, 1H), 7.88 (ddd, J = 7.9, 1.4, 0.6 Hz, 1H), 7.82 (m, 2H), 7.72 (d, J = 7.9 Hz, 1H), 7.31 (ddd, J = 7.6, 5.8, 1.5 Hz, 1H), 7.20 (s, 1H), 7.08 (s, 1H), 2.21 (s, 3H), 2.14 (s, 1H). ^{13}C NMR (125 MHz, D_2O): δ 162.3, 158.6, 150.8, 150.7, 142.1, 142.0, 141.3, 137.8, 134.4, 130.6, 130.4, 129.4, 129.3, 125.8, 125.2, 118.3, 18.6, 18.2. ESI–MS (m/z, MeOH): 679.0 (100%, [Ir(bpsa-PhdMe)Cl_2]$^-$).

Iridium *N*,*N*′-(naphthalene-2,3-diyl)bis(pyridine-2-sulfonamide) dichloride sodium salt (Na[Ir(bpsa-NPTH)Cl_2]) **5**. Yield: 32.4%, yellow powder. ^{1}H NMR (500 MHz, CD_3CN): δ 9.78 (dd, J = 5.7, 1.5 Hz, 1H), 8.27 (dt, J = 7.8, 1.4 Hz, 1H), 7.93 (m, 3H), 7.86 (ddd, J = 7.7, 5.7, 1.4 Hz, 1H), 7.74 (m, 2H), 7.72 (s, 1H), 7.69 (s, 1H), 7.63 (d, J = 8.2, 1H), 7.33 (m, 2H), 7.25 (ddd, J = 8.1, 6.9, 1.2 Hz, 1H). ^{13}C NMR (125 MHz, D_2O): δ 162.1, 158.5, 150.9, 150.7, 145.0, 142.2, 141.4, 139.7, 131.4, 130.6, 129.5, 129.1, 127.2, 126.3, 126.2, 126.1, 126.0, 124.9, 124.7, 113.2. ESI–MS (m/z, MeOH): 701.0 (100%, [Ir(bpsa-NPTH)Cl_2]$^-$).

2.3. Methods and techniques

2.3.1. Physical characterization

^{1}H and ^{13}C NMR spectra were recorded on Bruker Avance 500 MHz spectrometers at room temperature. ESI–MS was performed on Thermo-Fisher LCQ instrument with ~90 μM methanol solutions. 1% Trifluoroacetic acid was added for mass spectrometry of the ligands. Elemental analysis was conducted by Robertson Microlit Laboratories (Ledgewood, NJ).

2.3.2. Electrochemstry

Cyclic voltammograms were measured on a CH-Instruments Model 600C Electrochemical Analyzer using a glassy-carbon working electrode, a coiled-platinum counter electrode, and a silver-wire pseudoreference electrode. Solutions were prepared with 0.1 M tetrabutylammonium hexafluorophosphate (Fluka, electrochemical grade) as the supporting electrolyte for analysis in acetonitrile and ~2 mM corresponding Ir(III) bpsa complex. All solutions were purged with argon before taking each measurement. Ferrocene was added as an internal standard, and the oxidation half-wave potential of ferrocene standard was set to +0.40 V versus SCE. A scan rate of 0.1 V/s was used, starting from the positive scan unless further noted.

2.3.3. Dynamic oxygen evolution measurements

Typically, a solution of the iridium complex (1 mL) was injected into a sealed 40 mL EPA vial containing 10 mL of 0.36 M CAN solution buffered in 1 M HNO_3 that was degassed by argon. O_2 evolution was dynamically monitored with pressure transducer equipped on top of the sealed EPA vials as described in previous literature [42], and the end point of the reaction was verified by GC analysis.

For water oxidation experiments using sodium periodate ($NaIO_4$) as a sacrificial oxidant, 30 mL 19 mM unbuffered solution of the oxidant was placed in a sealed 40 mL EPA vial. A solution of the iridium complex (1 mL) was then injected into the EPA vial, and the reaction was monitored immediately after the addition of the catalyst. Similarly, the components of the headspace in each reaction vial were checked with GC at the end of the experiments.

2.3.4. DFT calculations

All DFT calculations were performed with Gaussian 09 using the B3LYP functional and LANL2DZ as the basis set. Default parameters and thresholds were used for gradient convergence. Geometry optimizations for all five Ir(III) bpsa complexes were carried out under no constraints in vacuum condition, yielding reasonable optimal coordinates and orbital energies.

3. Results and discussion

3.1. Catalytic activities

The structurally altered derivatives **2**–**5** as well as the parent complex **1** were explored side by side for catalytic water oxi-

Please cite this article in press as: M. Li, S. Bernhard, Synthetically tunable iridium(III) bis-pyridine-2-sulfonamide complexes as efficient and durable water oxidation catalysts, Catal. Today (2016), http://dx.doi.org/10.1016/j.cattod.2016.11.027

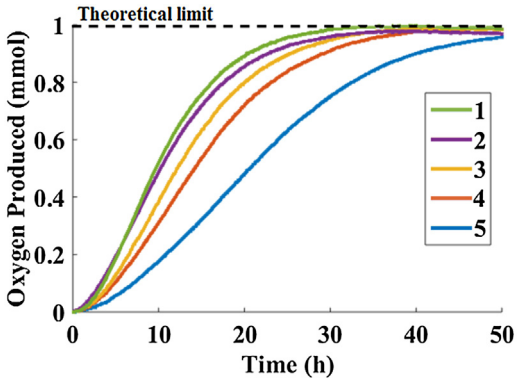

Fig. 2. O_2 evolution traces of complexes **1**–**5** at 50 μM catalyst and 0.36 M CAN (final volume = 11 mL). The total amount of O_2 produced with all catalysts is consistent with the stoichiometric limit of the added CAN.

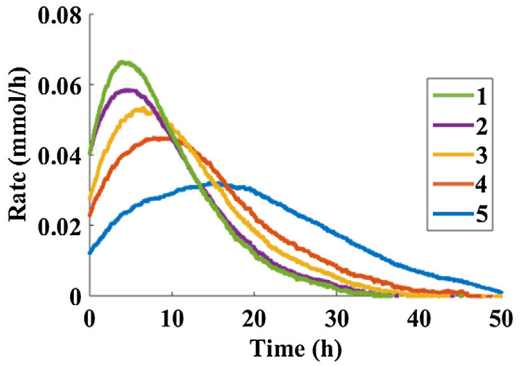

Fig. 3. O_2 evolution rates of complexes **1**–**5** over time at 50 μM catalyst and 0.36 M CAN (final volume = 11 mL).

dation that was chemically driven by cerium ammonium nitrate (CAN) buffered in 1 M HNO_3. O_2 evolution was monitored with the homebuilt pressure transducer setup as described previously [42], and the GC-verified results of these reactions are plotted in Fig. 2. Essentially all these reactions proceeded to completion, producing stoichiometric oxygen within 4% of the theoretical maximum yield. This finding is contrasted by recent work on iridium Cp* water oxidation catalysts that exhibit non-stoichiometric oxygen evolution at high catalyst loading [70–72]. No carbon dioxide was detected at the endpoint of these reactions. A short induction period when O_2 is initially evolved at a relatively slower rate was observed for all five complexes, corresponding to the exchange of the ancillary chloride ligands with labile water molecules from the solvent which was discussed in previously published work [49]. Monitoring the rate of O_2 evolution revealed that regardless of the added tuning groups, all substituted complexes **2**–**4** and complex **5** with the naphthalene linkage are similarly or slightly less active as water oxidation catalyst compared to the parent complex **1** (Fig. 3, Table S1). Complexes **2** and **3** with electro-withdrawing substituents (Cl and F respectively) catalyze water oxidation faster than **4** with the electron-donating substituents (Me); all the phenylene-linked complexes outperform **5** with the naphthalene linkage containing the extended conjugation system. Moreover, the maximum rate for **5** was achieved much later than for **1**–**4**, at a stage of the reaction when almost 40% CAN was already consumed. The distinct behaviors of these complexes observed in O_2 evolution trigger further in-depth studies to gain a better understanding of the effects of these structurally diverse ligands and, as a consequence, the mechanism of catalyzed water oxidation reactions.

3.2. Kinetics and mechanistic insights

The ratio of the Ce(IV) oxidant to the catalyst appear to have a strong effect on the catalytic mechanism [48,70,73]. Consequently, complexes **1**–**5** were further investigated as water oxidation catalysts with a large excess of CAN by varying the concentration of the catalyst over a wide range from 5 to 50 μM (Table S1, Fig. S1–S3). In contrast to the aforementioned results with a high catalyst load (50 μM), the amount of O_2 produced with all these complexes at relatively low catalyst concentrations was below the stoichiometric maximum yield, indicating a deactivation of the catalyst prior to the consumption of all CAN. Overall, the parent complex **1** exhibits superior performance compared to the structurally modified derivatives **2**–**5** as water oxidation catalysts. This is clearly documented by the fact that the TOF_{max} of **1** was up to one order of magnitude higher than those of **2**–**5**. Close inspection of the behaviors of these catalysts revealed that at lower concentrations the O_2 evolution lost the sigmoidal-like feature and appeared close to be linear over time, likely indicating a change in mechanisms when different CAN/catalyst ratios are involved.

For all complexes, the maximum O_2 evolution rate was found to be linearly correlated with catalyst concentration (Fig. 4A). A conventional log–log plot of maximum rate against the catalyst concentration exhibits an apparent order of one in catalyst for all these complexes (Fig. 4B), unlike the fractional reaction order observed in previous work with 0.80 M CAN [49]. Furthermore, the rate of oxygen evolution exhibited a notable increase (almost 10-fold) as compared to the results obtained for the parent complex **1** previously at high CAN concentration (Table S1) [49]. The concentration dependence on CAN as well as the variation in apparent reaction order in catalyst is consistent with mechanisms involving the formation of an intermediate containing Ce(IV) fragment as described in other iridium, ruthenium and iron water oxidation systems, [38,70,74–76] which further proves the non-innocence of CAN as a sacrificial oxidant under conditions involving high oxidant concentrations.

To evaluate the robustness of these complexes in water oxidation catalysis, long-term experiments were conducted for complexes **1**–**5** with a large excess of CAN at low catalyst concentrations (Fig. 5A, Fig. S3). Although these complexes generated oxygen below the stoichiometric limit, they remained constantly active for a week or more. **1** achieved the highest turnovers of up to 16,200 during this time, which was obtained in the presence of 71,210 equivalents of CAN (Table S1). **2** proved to be almost as durable and efficient as **1**, while **3**, which is also substituted with electron-withdrawing substituents, accomplished only about 80% of the turnovers of **2** (Fig. 5A). Complex **4** with the methyl substituents and **5** with the naphthalene linkage demonstrated robustness comparable to **3** (Fig. S3), with a slightly higher reactivity of observed for **4** under these conditions. Apparently, the kinetics profiles discussed above are not sufficient to understand the different TONs and evaluate the reactivity observed with different water oxidation catalysts. Nevertheless, interesting trends were found for complexes **1**–**5** when inspecting the relationship between the TOF_{max} and the molar ratio of CAN and catalyst (Fig. 5B, Fig. S4) [72]. Similar to the parent complex **1**, the TOF_{max} of **2** also peaked when the molar ratio between CAN and catalyst is around 18,000 with a 20 μM catalyst concentration, and it decreased slightly as the catalyst load was further reduced. The slightly lower turnovers obtained by **2** is likely due to the small reactivity difference between **1** and **2** (Fig. 5B). The TOF_{max} of **3** also reached a maximum at the same CAN/catalyst ratio as **1** and **2**, but a significant drop in reactivity was observed when the CAN/catalyst ratio was large (Fig. 5B). This difference in kinetics behaviors highlights the significant effect of the fluorine substituents on the reactivity of the catalyst. This decrease in reactivity is contrasted by the more robust nature of

Please cite this article in press as: M. Li, S. Bernhard, Synthetically tunable iridium(III) bis-pyridine-2-sulfonamide complexes as efficient and durable water oxidation catalysts, Catal. Today (2016), http://dx.doi.org/10.1016/j.cattod.2016.11.027

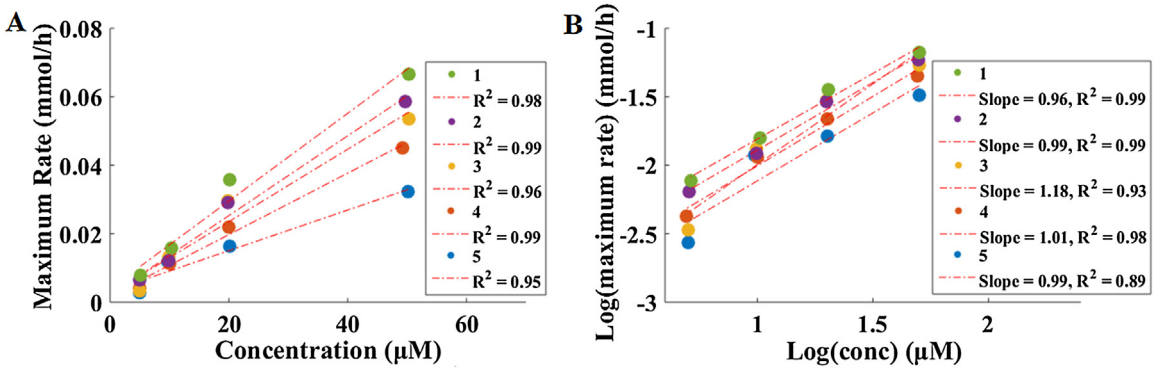

Fig. 4. A) Plots of maximum rates of O_2 evolution versus concentrations of complexes **1**–**5** at 0.36 M CAN (final volume = 11 mL). B) Log-log plot of complexes **1**–**5** and their linear fits. The slopes indicate the apparent orders of O_2 evolution on each catalyst.

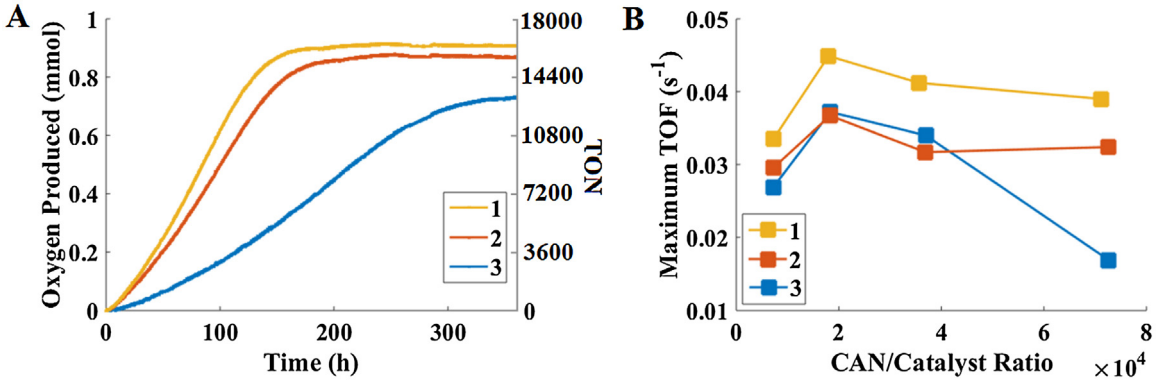

Fig. 5. A) Long-term O_2 evolution from 11 mL aqueous solutions of 5 μM complexes **1**–**3** and 0.36 M CAN. B) Trends of maximum TOF versus the molar ratio between CAN and catalyst for complexes **1**–**3**. The results for complex **4** and complex **5** are included in the Supporting information.

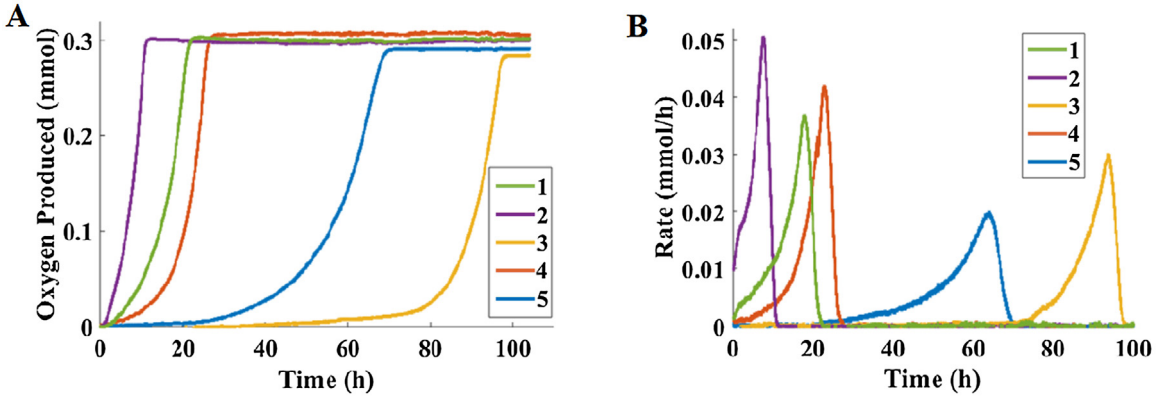

Fig. 6. A) O_2 evolution traces of complexes **1**–**5** at 5 μM catalyst and 19 mM $NaIO_4$ (final volume = 31 mL). Stoichiometric amount of oxygen was produced for all these complexes after an incubation time of various lengths. B) O_2 evolution rates of complexes **1**–**5** over time at 5 μM catalyst and 19 mM $NaIO_4$ (final volume = 31 mL).

the fluorinated version of the original $[Ir(ppy)_2(H_2O)_2]^+$ water oxidation catalyst [42], indicating a difference in the formation of the active catalytic species. Examining the dependence of TOF_{max} on CAN/catalyst ratio for complex **4** and **5** also revealed a similar prominent decrease in O_2 evolution rate as observed for **3** when CAN was present in great excess (Fig. S4). The decreased stability can easily be attributed to the addition of the methyl substituents or the extension of conjugation system in the linkage moiety that decreases its resilience to oxidative degradation. Moreover, **4** and **5** reached their maximum TOF_{max} at larger CAN/catalyst ratios than **1**, **2** and **3**, suggesting that two different catalyst degradation pathways may be involved for these five bpsa complexes.

Established as efficient and durable water oxidation catalysts operating under highly oxidative and acidic conditions, complexes **1**–**5** were also investigated for water oxidation catalysis with $NaIO_4$ acting as a two-electron oxidant. While it typically requires isotope study to determine the source of oxygen during water oxidation processes, periodate is stable over a wide pH range (approximately from 2 to 7.5), which allows us to explore the behaviors of these water oxidation catalysts in a near-neutral reaction medium [77]. Under conditions of low catalyst concentration and small excess of oxidant, the maximum TOFs achieved for complexes **1**–**5** are generally up to three times as fast as those observed under similar conditions with CAN as the primary oxidant (Fig. 6, Table S2). It

Please cite this article in press as: M. Li, S. Bernhard, Synthetically tunable iridium(III) bis-pyridine-2-sulfonamide complexes as efficient and durable water oxidation catalysts, Catal. Today (2016), http://dx.doi.org/10.1016/j.cattod.2016.11.027

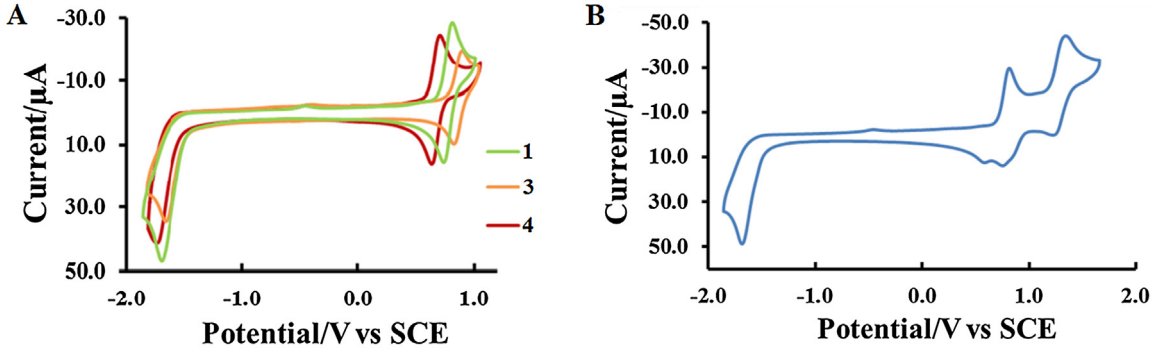

Fig. 7. A) Cyclic voltammograms of complexes **1**, **3** and **4** in acetonitrile to demonstrate the reversible oxidation process associated with Ir(IV)/Ir(III) redox couple of each complex in the absence of water. The results for complex **2** and complex **5** are included in the Supporting information. B) Cyclic voltammograms of complex **1** in acetonitrile with a more positive limit. For all CVs, a glassy carbon working electrode was used with a 0.1 M tetra-*n*-butylammonium hexafluorophosphate (TBAH) supporting electrolyte solution. Scan rate = 0.1 V/s.

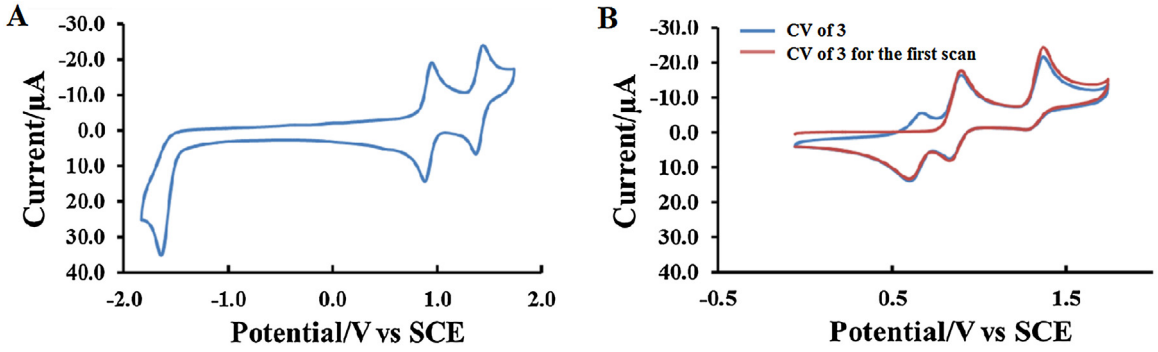

Fig. 8. Cyclic voltammograms of complex **2** (A) and complex **3** (B) in acetonitrile. A glassy carbon working electrode was used with a 0.1 M tetra-*n*-butylammonium hexafluorophosphate (TBAH) supporting electrolyte solution. Scan rate = 0.1 V/s.

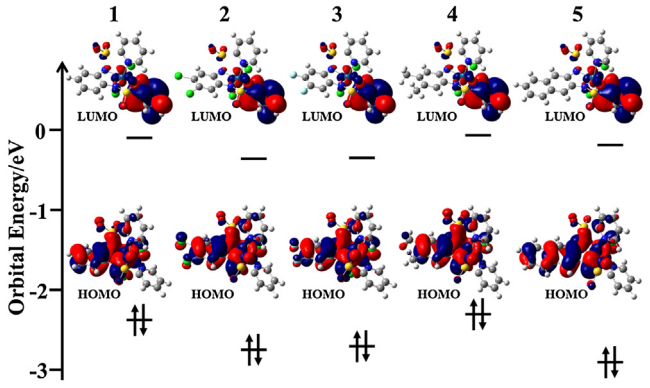

Fig. 9. Frontier orbitals for complexes **1**–**5** based on DFT calculations (B3LYP/LANL2DZ). The HOMO orbital energies of these complexes can be tuned by addition of electron-donating or electron-withdrawing substituents due to the mixed metal/ligand character of these orbitals. The enlarged π-system of **5** changes the electronic structure of this complex dramatically, and thus a direct comparison with the phenylene-bridged system is impossible.

is notable that the time of incubation was markedly longer compared to CAN-driven water oxidation, especially in the case of **3** and **5**, as evidenced by the bifurcation time t_B extracted from the O_2 evolution traces. The extremely long induction period followed by rapid O_2 generation could be an indication of the formation of iridium oxide nanoparticles. However, clear differences in bifurcation time as well as O_2 evolution rate among these bpsa complexes with diverse substituents were observed, suggesting a ligand effect on an active molecular species. Besides, the fact that the reaction rates are of the same order as the analogous molecular iridium water oxidation catalysts, which is roughly one order of magnitude less than the typical heterogeneous systems, [78,79] also points toward the molecular nature of these water oxidation catalysts. An alternative explanation for the delayed onset of these reactions could be the differences in $Cl^-/H_2O/IO_4^-$ substitution initiated by periodate oxidation. The sigmoid shape of the O_2 evolution traces observed using $NaIO_4$ as the oxidant is typical for autocatalytic reactions, [80–82] which evokes complimentary insights into water oxidation mechanisms and further highlights the distinct roles of the sacrificial oxidants in the catalytic cycle.

3.3. Electrochemistry and DFT modeling

Cyclic voltammetry (CV) in acetonitrile was used to evaluate the redox properties of complexes **1**-**5**, providing valuable insights into the effect of various substituents on the electronic structure of Ir(III) bpsa complexes. The reversible oxidation wave, which can be assigned to the Ir(IV)/Ir(III) redox couple, was observed for all five complexes at potentials ranging from +0.64 V to +0.92 V versus SCE (Fig. 7A, Fig. S5, Table 1). Analogous to the parent complex **1** (Fig. 7B), the CVs of **2**, **3** and **4** show a second reversible oxidation process at more positive potentials that was assigned to the oxidation of the phenylene linkage as discussed in the previous work [49]. Moreover, **3** demonstrates an additional reversible oxidation wave at a potential lower than the Ir(IV)/Ir(III) redox couple after a complete oxidative sweep to potential past the second oxidation. This is likely due to the formation of a degradation product caused by the introduction of more labile fluorine substituents to the bridging unit (Fig. 8B). For complex **4**, the methyl substituents are believed to undergo some irreversible transformation at high oxidation potential as evidenced by the irreversible oxidation peak at +1.63 V versus

Please cite this article in press as: M. Li, S. Bernhard, Synthetically tunable iridium(III) bis-pyridine-2-sulfonamide complexes as efficient and durable water oxidation catalysts, Catal. Today (2016), http://dx.doi.org/10.1016/j.cattod.2016.11.027

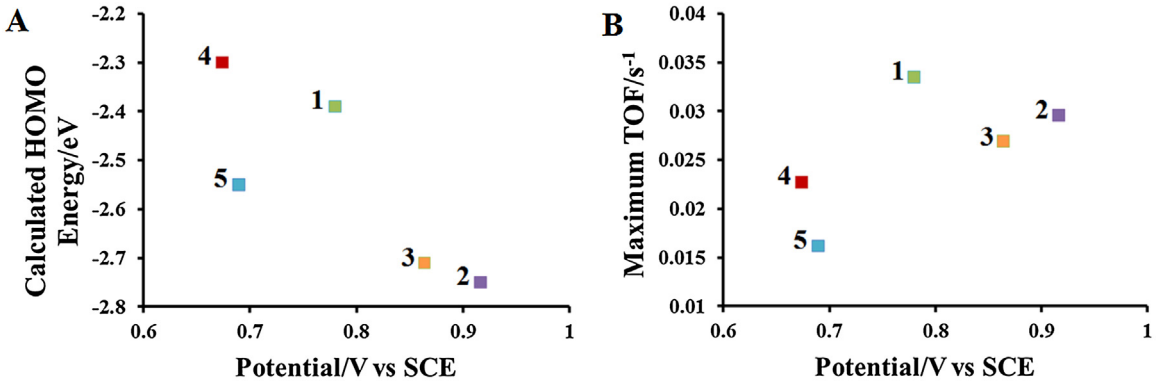

Fig. 10. A) Relationship between the oxidation potentials of complexes **1**–**5** in acetonitrile measured by cyclic voltammetry and calculated HOMO energies from DFT calculation (B3LYP/LANL2DZ). B) Relationship between the oxidation potentials of complexes **1**–**5** in acetonitrile measured by cyclic voltammetry and maximum TOFs determined at 50 μM catalyst and 0.36 M CAN.

Table 1
Electrochemical properties[a] of complexes **1**–**5**.

Complex	$E_{1/2}^{OX}$/V (ΔE^b/mV)			E_{pc}^{RED}/V
1	+0.78 (75)	+1.28 (90)	–	−1.70
2	+0.92 (69)	+1.41 (67)	–	−1.64
3	+0.64 (73)[c]	+0.86 (68)	+1.32 (95)	−1.66
4	+0.67 (71)	+1.15 (92)	+1.63[d]	−1.71
5	+0.69 (49)[e]	+1.31[e]	+1.50[e]	−1.86

[a] Measured in MeCN containing 0.1 M tetra-*n*-butylammonium hexafluorophosphate (TBAH) solution as the electrolyte. Scan rate = 0.1 V/s. All potentials were referenced to SCE using ferrocene as an internal standard (fc/fc^+ = +0.40 V vs SCE).
[b] Peak separation.
[c] A reversible oxidation peak at +0.64 V, due to the formation of a degradation product of the original complex, is observed if **3** is oxidized after an oxidative sweep to +1.9 V (Fig. 8B).
[d] The irreversible oxidation peak corresponding to the oxidation of the methyl substituents appears if **4** is oxidized to +1.9 V (Fig. S6).
[e] The redox behaviors of **5** with naphthalene linkage differ from **1** containing phenylene linkage: two adjacent, irreversible oxidation peaks due to the oxidation of the ligand's bridging unit are observed (Fig. S7). Also, the relatively small peak separation of the oxidative process of Ir(IV)/Ir(III) redox couple indicates a difference in oxidation mechanism.

SCE (Fig. S6). The susceptibility of the methyl groups to degradation has also been observed in other molecular water oxidation catalysts with various ligand scaffolds. It is noteworthy that **2** did not undergo irreversible transformations upon the oxidative sweep as evidenced by the two fully reversible oxidation peaks in CV (Fig. 8A). The observed electronic stability caused by the addition of the chlorine substituents to the phenylene bridging unit is consistent with the previously observed great robustness of **2** as a water oxidation catalyst, which explains the high TONs in the longevity experiments under highly acidic and oxidative conditions. Not surprisingly, complex **5**, containing the naphthalene linkage, exhibits electrochemical properties distinctly different than its cousin complexes **1**–**4**. The oxidation wave corresponding to Ir(IV)/Ir(III) redox couple at +0.69 V versus SCE turned out to be quasi-reversible with much smaller peak separation which was followed by two adjoining irreversible oxidation peaks caused by the oxidation of the ligand's bridging unit (Fig. S5, Fig. S7) [83].

The observed effect of the redox behavior of these bpsa complexes caused by adding electron-donating or electron-withdrawing substituents to the linkage moiety is reasonably predictable by correlation with the DFT calculated HOMO energy levels of these complexes. As illustrated in Fig. 9, the calculated HOMOs for complexes **1**-**5** all exhibit a significant distribution of electron density over both the metal center and the bridging unit, which is in good agreement with the presence of an oxidation process beyond the Ir(IV)/Ir(III) redox couple observed electrochemically. The involvement of the ligand in the oxidation process allows the fine-tuning of the energy of HOMO, which is strongly involved in water oxidation catalysis. The addition of electron-withdrawing substituents was found to stabilize the HOMO, which greatly impedes the oxidation process as evidenced by the exceptionally high redox potential of the Ir(IV)/Ir(III) couple. On the other hand, the addition of electron-donating substituents causes the opposite effect (Fig. 10A).

It is expected that electron-donating substituents greatly facilitate the oxidation process through the electronic destabilization of the HOMO of the bpsa complexes. Accordingly, complex **4** with the higher HOMO energy is expected to be more easily oxidized and thus catalyze water oxidation faster than the parent complex **1** due to the easier accessibility of the highly oxidized species that are required for the abstraction of electrons from water. In reality, poor activity was observed for **4** (Fig. 10B), which can be attributed to the limited driving force provided by the oxidized species as well as the electronic instability caused by the possible destructive transformation of the methyl groups under the highly oxidative conditions (Fig. S6). For complexes **2** and **3**, which are decorated with electron-withdrawing substituents, the stabilization of the HOMO of the complex effectively enlarges the energy difference between the ground state and the first oxidized state, rendering it a stronger oxidant and thus potentially a more efficient water oxidation catalyst compared to the parent complex **1**. However, the high energy barrier needed for reaching the required highly oxidized state of the catalyst significantly impedes the water oxidation process, and as a result, both **2** and **3** perform worse than **1** (Fig. 10). It is worth mentioning that the reactivity of complex **5** appears to be the worst among all these complexes, likely due to the fact that the bridging unit of **5** is most susceptible to oxidation as illustrated by the irreversibility of the oxidative processes evidenced by the measured CV (Fig. S7).

4. Conclusions

A variety of iridium bis-pyridine-2-sulfonamide (bpsa) complexes with diverse substituents on the phenylene bridging unit as well as an iridium complex with a new bpsa ligand containing the naphthalene linkage were synthesized and studied in the homogeneous, chemically driven oxidation of water. The electronic structure of these iridium water oxidation catalysts is highly tunable through substitution with electron-donating or electron-withdrawing substituents, which is documented by cyclic voltammetry and DFT calculations. Such differences in the electronic structures of these complexes lead to significantly different activity in water oxidation catalysis. Very different kinetic behaviors are observed for these complexes, suggesting that various

Please cite this article in press as: M. Li, S. Bernhard, Synthetically tunable iridium(III) bis-pyridine-2-sulfonamide complexes as efficient and durable water oxidation catalysts, Catal. Today (2016), http://dx.doi.org/10.1016/j.cattod.2016.11.027

mechanistic pathways are involved. Moreover, it has been found that the reactivity of these water oxidation catalysts is affected by many other factors including the driving force provided by the oxidized catalyst, the accessibility of highly oxidized species, and the electronic stability of the involved catalyst. These factors need be balanced when designing a feasible water oxidation catalyst in order to achieve optimal performance. Future work will involve further exploration of these water oxidation catalysts under various conditions and precise detection of the key intermediates to gain an in-depth understanding of the catalytic mechanisms.

Acknowledgement

The authors acknowledge support from the National Science Foundation through CHE-1362629.

Appendix A. Supplementary data

Supplementary data associated with this article can be found, in the online version, at http://dx.doi.org/10.1016/j.cattod.2016.11.027.

References

[1] B.H. Farnum, K.-R. Wee, T.J. Meyer, Nat. Chem. (2016), http://dx.doi.org/10.1038/nchem.2536.
[2] A. Polman, M. Knight, E.C. Garnett, B. Ehrler, W.C. Sinke, Science 352 (2016) 307.
[3] D. Gust, T.A. Moore, A.L. Moore, Acc. Chem. Res. 34 (2001) 40–48.
[4] M. Law, L.E. Greene, J.C. Johnson, R. Saykally, P. Yang, Nat. Mater. 4 (2005) 455–459.
[5] N.D. McDaniel, S. Bernhard, Dalton Trans. 39 (2010) 10021–10030.
[6] N.S. Lewis, D.G. Nocera, Proc. Natl. Acad. Sci. USA 103 (2006) 15729–15735.
[7] D. Gust, T.A. Moore, A.L. Moore, Acc. Chem. Res. 42 (2009) 1890–1898.
[8] S.C. Roy, O.K. Varghese, M. Paulose, C.A. Grimes, ACS Nano 4 (2010) 1259–1278.
[9] A.J. Morris, G.J. Meyer, E. Fujita, Acc. Chem. Res. 42 (2009) 1983–1994.
[10] L. Chen, Z. Guo, X.-G. Wei, C. Gallenkamp, J. Bonin, E. Anxolabéhère-Mallart, K.-C. Lau, T.-C. Lau, M. Robert, J. Am. Chem. Soc. 137 (2015) 10918–10921.
[11] A. Dhakshinamoorthy, A.M. Asiri, H. García, Angew. Chem. Int. Ed. 55 (2016) 5414–5445.
[12] A. Kudo, Y. Miseki, Chem. Soc. Rev. 38 (2009) 253–278.
[13] M.G. Walter, E.L. Warren, J.R. McKone, S.W. Boettcher, Q. Mi, E.A. Santori, N.S. Lewis, Chem. Rev. 110 (2010) 6446–6473.
[14] V. Artero, M. Chavarot-Kerlidou, M. Fontecave, Angew. Chem. Int. Ed. 50 (2011) 7238–7266.
[15] J. Liu, Y. Liu, N. Liu, Y. Han, X. Zhang, H. Huang, Y. Lifshitz, S.-T. Lee, J. Zhong, Z. Kang, Science 347 (2015) 970–974.
[16] F. Li, K. Fan, B. Xu, E. Gabrielsson, Q. Daniel, L. Li, L. Sun, J. Am. Chem. Soc. 137 (2015) 9153–9159.
[17] P.N. Curtin, L.L. Tinker, C.M. Burgess, E.D. Cline, S. Bernhard, Inorg. Chem. 48 (2009) 10498–10506.
[18] Y. Fu, D. Sun, Y. Chen, R. Huang, Z. Ding, X. Fu, Z. Li, Angew. Chem. Int. Ed. 51 (2012) 3364–3367.
[19] C.D. Windle, R.N. Perutz, Coord. Chem. Rev. 256 (2012) 2562–2570.
[20] S. Sato, T. Morikawa, S. Saeki, T. Kajino, T. Motohiro, Angew. Chem. Int. Ed. 49 (2010) 5101–5105.
[21] J.M. Smieja, M.D. Sampson, K.A. Grice, E.E. Benson, J.D. Froehlich, C.P. Kubiak, Inorg. Chem. 52 (2013) 2484–2491.
[22] M.Y. Azwar, M.A. Hussain, A.K. Abdul-Wahab, Renew. Sustain. Energy Rev. 31 (2014) 158–173.
[23] A.V. Nguyen, S.R. Thomas-Hall, A. Malnoē, M. Timmins, J.H. Mussgnug, J. Rupprecht, O. Kruse, B. Hankamer, P.M. Schenk, Eukaryot. Cell 7 (2008) 1965–1979.
[24] Y.V. Tolmachev, Russ. J. Electrochem. 50 (2014) 301–316.
[25] J. Du, Z. Chen, C. Chen, T.J. Meyer, J. Am. Chem. Soc. 137 (2015) 3193–3196.
[26] G. Zhang, S.K. Hanson, Org. Lett. 15 (2013) 650–653.
[27] W. Song, A.K. Vannucci, B.H. Farnum, A.M. Lapides, M.K. Brennaman, B. Kalanyan, L. Alibabaei, J.J. Concepcion, M.D. Losego, G.N. Parsons, T.J. Meyer, J. Am. Chem. Soc. 136 (2014) 9773–9779.
[28] M.D. Kärkäs, O. Verho, E.V. Johnston, B. Åkermark, Chem. Rev. 114 (2014) 11863–12001.
[29] J.D. Blakemore, R.H. Crabtree, G.W. Brudvig, Chem. Rev. 115 (2015) 12974–13005.
[30] S.W. Gersten, G.J. Samuels, T.J. Meyer, J. Am. Chem. Soc. 104 (1982) 4029–4030.
[31] S.R. Cooper, M. Calvin, J. Am. Chem. Soc. 99 (1977) 6623–6630.
[32] Y. Gao, R.H. Crabtree, G.W. Brudvig, Inorg. Chem. 51 (2012) 4043–4050.
[33] C. Sens, I. Romero, M. Rodriguez, A. Llobet, T. Parella, J. Benet-Buchholz, J. Am. Chem. Soc. 126 (2004) 7798–7799.
[34] Y. Xu, A. Fischer, L. Duan, L. Tong, E. Gabrielsson, B. Åkermark, L. Sun, Angew. Chem. Int. Ed. 49 (2010) 8934–8937.
[35] N.S. McCool, D.M. Robinson, J.E. Sheats, G.C. Dismukes, J. Am. Chem. Soc. 133 (2011) 11446–11449.
[36] A. Sartorel, M. Bonchio, S. Campagna, F. Scandola, Chem. Soc. Rev. 42 (2013) 2262–2280.
[37] K.J. Young, M.K. Takase, G.W. Brudvig, Inorg. Chem. 52 (2013) 7615–7622.
[38] L. Duan, F. Bozoglian, S. Mandal, B. Stewart, T. Privalov, A. Llobet, L. Sun, Nat. Chem. 4 (2012) 418–423.
[39] L. Bernet, R. Lalrempuia, W. Ghattas, H. Müller-Bunz, L. Vigara, A. Llobet, M. Albrecht, Chem. Commun. 47 (2011) 8058–8060.
[40] N. Kaveevivitchai, R. Zong, H.-W. Tseng, R. Chitta, R.P. Thummel, Inorg. Chem. 51 (2012) 2930–2939.
[41] J.J. Concepcion, J.W. Jurss, J.L. Templeton, T.J. Meyer, J. Am. Chem. Soc. 130 (2008) 16462–16463.
[42] N.D. McDaniel, F.J. Coughlin, L.L. Tinker, S. Bernhard, J. Am. Chem. Soc. 130 (2008) 210–217.
[43] J.D. Blakemore, N.D. Schley, D. Balcells, J.F. Hull, G.W. Olack, C.D. Incarvito, O. Eisenstein, G.W. Brudvig, R.H. Crabtree, J. Am. Chem. Soc. 132 (2010) 16017–16029.
[44] R. Lalrempuia, N.D. McDaniel, H. Müller-Bunz, S. Bernhard, M. Albrecht, Angew. Chem. Int. Ed. 49 (2010) 9765–9768.
[45] A. Savini, A. Bucci, G. Bellachioma, S. Giancola, F. Palomba, L. Rocchigiani, A. Rossi, M. Suriani, C. Zuccaccia, A. Macchioni, J. Organomet. Chem. 771 (2014) 24–32.
[46] C. Wang, J.-L. Wang, W. Lin, J. Am. Chem. Soc. 134 (2012) 19895–19908.
[47] D.G.H. Hetterscheid, J.N.H. Reek, Chem. Commun. 47 (2011) 2712–2714.
[48] J.A. Woods, R. Lalrempuia, A. Petronilho, N.D. McDaniel, H. Müller-Bunz, M. Albrecht, S. Bernhard, Energy Environ. Sci. 7 (2014) 2316–2328.
[49] M. Li, K. Takada, J.I. Goldsmith, S. Bernhard, Inorg. Chem. 55 (2016) 518–526.
[50] M. Navarro, M. Li, H. Müller-Bunz, S. Bernhard, M. Albrecht, Chem. Eur. J. 22 (2016) 6740–6745.
[51] W.C. Ellis, N.D. McDaniel, S. Bernhard, T.J. Collins, J. Am. Chem. Soc. 132 (2010) 10990–10991.
[52] J.L. Fillol, Z. Codolà, I. Garcia-Bosch, L. Gómez, J.J. Pla, M. Costas, Nat. Chem. 3 (2011) 807–813.
[53] M.K. Coggins, M.-T. Zhang, A.K. Vannucci, C.J. Dares, T.J. Meyer, J. Am. Chem. Soc. 136 (2014) 5531–5534.
[54] B. Zhang, F. Li, F. Yu, H. Cui, X. Zhou, H. Li, Y. Wang, L. Sun, Chem. Asian J. 9 (2014) 1515–1518.
[55] D. Wang, J.T. Groves, Proc. Natl. Acad. Sci. U. S. A. 110 (2013) 15579–15584.
[56] Q. Yin, J.M. Tan, C. Besson, Y.V. Geletii, D.G. Musaev, A.E. Kuznetsov, Z. Luo, K.I. Hardcastle, C.L. Hill, Science 328 (2010) 342–345.
[57] D.J. Wasylenko, R.D. Palmer, E. Schott, C.P. Berlinguette, Chem. Commun. 48 (2012) 2107–2109.
[58] S.M. Barnett, K.I. Goldberg, J.M. Mayer, Nat. Chem. 4 (2012) 498–502.
[59] M.-T. Zhang, Z. Chen, P. Kang, T.J. Meyer, J. Am. Chem. Soc. 135 (2013) 2048–2051.
[60] T. Zhang, C. Wang, S. Liu, J.-L. Wang, W. Lin, J. Am. Chem. Soc. 136 (2014) 273–281.
[61] J.F. Hull, D. Balcells, J.D. Blakemore, C.D. Incarvito, O. Eisenstein, G.W. Brudvig, R.H. Crabtree, J. Am. Chem. Soc. 131 (2009) 8730–8731.
[62] A. Bucci, A. Savini, L. Rocchigiani, C. Zuccaccia, S. Rizzato, A. Albinati, A. Llobet, A. Macchioni, Organometallics 31 (2012) 8071–8074.
[63] A. Savini, G. Bellachioma, S. Bolaño, L. Rocchigiani, C. Zuccaccia, D. Zuccaccia, A. Macchioni, ChemSusChem 5 (2012) 1415–1419.
[64] C. Zuccaccia, G. Bellachioma, S. Bolaño, L. Rocchigiani, A. Savini, A. Macchioni, Eur. J. Inorg. Chem. (2012) 1462–1468.
[65] A. Savini, P. Belanzoni, G. Bellachioma, C. Zuccaccia, D. Zuccaccia, A. Macchioni, Green Chem. 13 (2011) 3360–3374.
[66] C. Zuccaccia, G. Bellachioma, O. Bortolini, A. Bucci, A. Savini, A. Macchioni, Chem. Eur. J. 20 (2014) 3446–3456.
[67] J.D. Blakemore, N.D. Schley, G.W. Olack, C.D. Incarvito, G.W. Brudvig, R.H. Crabtree, Chem. Sci. 2 (2011) 94–98.
[68] D.B. Grotjahn, D.B. Brown, J.K. Martin, D.C. Marelius, M.-C. Abadjian, H.N. Tran, G. Kalyuzhny, K.S. Vecchio, Z.G. Specht, S.A. Cortes-Llamas, V. Miranda-Soto, C. van Niekerk, C.E. Moore, A.L. Rheingold, J. Am. Chem. Soc. 133 (2011) 19024–19027.
[69] U. Hintermair, S.M. Hashmi, M. Elimelech, R.H. Crabtree, J. Am. Chem. Soc. 134 (2012) 9785–9795.
[70] A. Bucci, G. Menendez Rodriguez, G. Bellachioma, C. Zuccaccia, A. Poater, L. Cavallo, A. Macchioni, ACS Catal. 6 (2016) 4559–4563.
[71] A. Savini, A. Bucci, G. Bellachioma, L. Rocchigiani, C. Zuccaccia, A. Llobet, A. Macchioni, Eur. J. Inorg. Chem. 4 (2014) 690–697.
[72] I. Corbucci, A. Petronilho, H. Müller-Bunz, L. Rocchigiani, M. Albrecht, A. Macchioni, ACS Catal. 5 (2015) 2714–2718.
[73] M. Yoshida, S. Masaoka, J. Abe, K. Sakai, Chem. Asian J. 5 (2010) 2369–2378.
[74] A. Kimoto, K. Yamauchi, M. Yoshida, S. Masaoka, K. Sakai, Chem. Commun. 48 (2012) 239–241.
[75] Z. Codolà, I. Garcia-Bosch, F. Acuña-Parés, I. Prat, J.M. Luis, M. Costas, J. Lloret-Fillol, Chem. Eur. J. 19 (2013) 8042–8047.
[76] Z. Codolà, L. Gomez, S.T. Kleespies, L. Que, M. Costas, J. Lloret-Fillol, Nat. Commun. Nat. Comm. 6 (2015) 5865.
[77] A.R. Parent, R.H. Crabtree, G.W. Brudvig, Chem. Soc. Rev. 42 (2013) 2247–2252.

Please cite this article in press as: M. Li, S. Bernhard, Synthetically tunable iridium(III) bis-pyridine-2-sulfonamide complexes as efficient and durable water oxidation catalysts, Catal. Today (2016), http://dx.doi.org/10.1016/j.cattod.2016.11.027

[78] A.R. Parent, T.P. Brewster, W. De Wolf, R.H. Crabtree, G.W. Brudvig, Inorg. Chem. 51 (2012) 6147–6152.
[79] A.R. Parent, J.D. Blakemore, G.W. Brudvig, R.H. Crabtree, Chem. Commun. 47 (2011) 11745–11747.
[80] J.I. Steinfeld, J.S. Francisco, W.L. Hase, Chemical Kinetics and Dynamics, 2nd ed., Prentice-Hall, 1999, pp. 151–152.
[81] R.A. Adigun, M. Mhike, W. Mbiya, S.B. Jonnalagadda, R.H. Simoyi, J. Phys. Chem. A. 118 (2014) 2196–2208.
[82] C.-X. Yin, Y. Sasaki, R.G. Finke, Inorg. Chem. 44 (2005) 8521–8530.
[83] R.E. Sioda, B. Frankowska, J. Electroanal. Chem. 612 (2008) 147–150.

Please cite this article in press as: M. Li, S. Bernhard, Synthetically tunable iridium(III) bis-pyridine-2-sulfonamide complexes as efficient and durable water oxidation catalysts, Catal. Today (2016), http://dx.doi.org/10.1016/j.cattod.2016.11.027